Title	Angular dependence of columnar recombination in high pressure xenon gas using time profiles of scintillation emission
Author(s)	Nakamura, K.D.; Ban, S.; Hirose, M.; Ichikawa, A.K.; Ishiyama, Y.; Minamino, A.; Miuchi, K.; Nakaya, T.; Sekiya, H.; Tanaka, S.; Ueshima, K.
Citation	Journal of Instrumentation (2018), 13
Issue Date	2018-07
URL	http://hdl.handle.net/2433/235153
Right	© 2018 The Author(s). Published by IOP Publishing Ltd on behalf of Sissa Medialab. Original content from this work may be used under the terms of the Creative Commons Attribution 3.0 licence. Any further distribution of this work must maintain attribution to the author(s) and the title of the work, journal citation and DOI.
Type	Journal Article
Textversion	publisher

Journal of Instrumentation

Angular dependence of columnar recombination in high pressure xenon gas using time profiles of scintillation emission

Published by IOP Publishing for Sissa Medialab

Received: *March 16, 2018*
Accepted: *July 9, 2018*
Published: *July 20, 2018*

Angular dependence of columnar recombination in high pressure xenon gas using time profiles of scintillation emission

K.D. Nakamura,[a,1] **S. Ban,**[b] **M. Hirose,**[b] **A.K. Ichikawa,**[b] **Y. Ishiyama,**[b] **A. Minamino,**[b] **K. Miuchi,**[a] **T. Nakaya,**[b] **H. Sekiya,**[c] **S. Tanaka**[b] **and K. Ueshima**[d]

[a] *Kobe University,*
Rokkodai, Nada-ku Kobe-shi, Hyogo, 657-8501, Japan
[b] *Kyoto University,*
Kitashirakawaoiwake-cho Sakyo-ku Kyoto-shi Kyoto, 606-8502, Japan
[c] *Kamioka Observatory, ICRR, The University of Tokyo,*
456 Higashimozumi Kamioka-cho Hida-shi Gifu, 506-1205, Japan
[d] *RCNS, Tohoku University,*
6-3 Aramakiazaaoba, Aoba-ku Sendai-shi, Miyagi, 980-8578, Japan

E-mail: kiseki@harbor.kobe-u.ac.jp

Abstract: The angular dependence of columnar recombination in xenon (Xe) gas, if observed for low energy nuclear tracks, can be used for a direction-sensitive dark matter search. We measured both scintillation and ionization yields to study columnar recombination for 5.4 MeV alpha particles in a high pressure gas detector filled with Xe gas at a pressure of 8 atm. Because the recombination photons are emitted several microseconds after de-excitation, the scintillation photons are separated into fast and slow components. While the fast component is not dependent on the track angle relative to the drift electric field, the slow component increases when the track is aligned with the electric field. This result indicates that the track angle relative to the electric field can be reconstructed from the scintillation time profile.

Keywords: Dark Matter detectors (WIMPs, axions, etc.); Gaseous detectors; Noble liquid detectors (scintillation, ionization, double-phase); Time projection Chambers (TPC)

ArXiv ePrint: 1803.00752

[1] Corresponding author.

https://doi.org/10.1088/1748-0221/13/07/P07015

2018 JINST 13 P07015

Contents

2018 JINST 13 P07015

1 Introduction

A possibility of application of columnar recombination in high-pressure xenon (Xe) gas to the direction-sensitive dark matter search was raised by D. R. Nygren in 2013 [1]. Columnar recombination is a phenomenon in which the recombination of electrons and ions distributed in a columnar form along the path of a charged particle increases when the electric field and column are oriented in a parallel manner in a time-projection chamber (TPC). For Xe with a density of 0.05 g/cm^3 ($\sim$ 10 atm), an Onsager radius of 70 nm, and a 30 keV nuclear-recoil track length of 2100 nm, a large aspect ratio of 30 times is expected [1]. If the columnar recombination signal is significant and measurable, the angle with respect to the applied electric field can be reconstructed, for example, by comparing yields of scintillation and ionization. A direction-sensitive dark matter search with a large target mass and spin-independent sensitivity would be possible if it is conducted with high-pressure Xe gas. In a previous study carried out by the NEXT group, trimethylamine and Xe gases were mixed to quickly thermalize ionization electrons and enhance the Penning effect. A correlation between the measured charge and the angle of α-particle tracks was observed [2], but the scintillation emission was strongly suppressed [3]. This observation led to the conclusion that it is difficult to apply this approach to a direction-sensitive dark matter search. In this study, we used the time profile of scintillation emission from pure Xe gas to enhance the sensitivity to columnar recombination. Because the recombinations and resulting photon emissions would occur during electron drift, it is expected that the timescale is several μs and much slower than the de-excitation emission. We conducted an experiment to quantify this effect with a small detector and measured its dependence on the track angle using 5.4 MeV α-particle tracks.

2 Experimental setup

As depicted in figure 1, a detector is constructed in a vessel filled with 8 atm Xe gas. The detector has a 5-mm-thick drift region and a 2-mm-thick electroluminescence (EL) region where a high electric field is applied to measure the ionization signal via EL photon detection. A vacuum ultraviolet

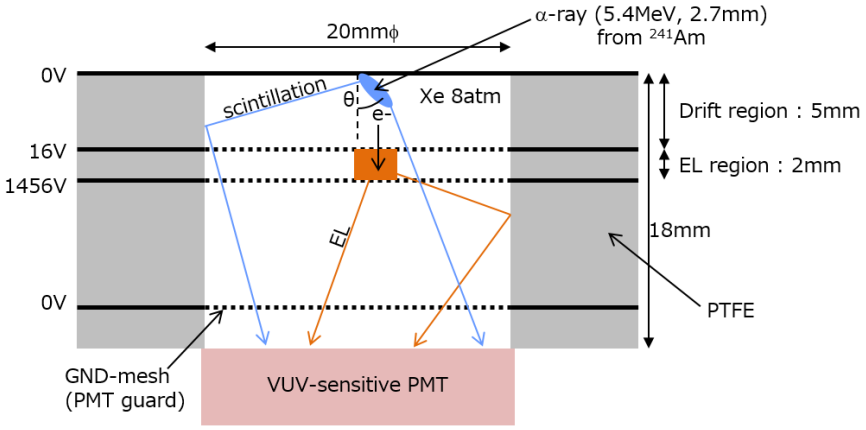

Figure 1. Schematic of the detector.

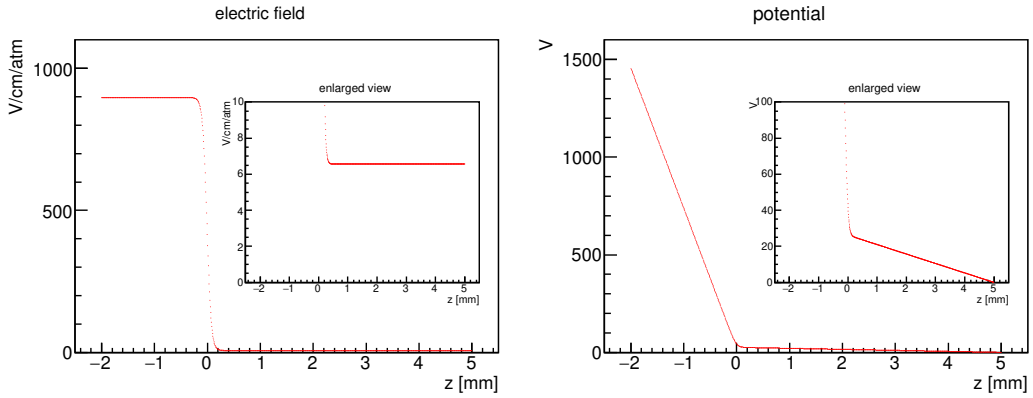

Figure 2. Electric field and potential in the detector, as calculated using the three-dimensional finite-element mesh generator gmsh [4] and Elmer [5]. The drift top, drift mesh and EL mesh correspond to $z = 5$ mm, 0 mm, and -2 mm, respectively. 0 V, +16 V and +1456 V are applied to the drift top, drift mesh and EL mesh, respectively. In the gmsh simulation, the mesh is constructed as wires arranged in x and y directions.

(VUV)-sensitive photomultiplier tube (PMT)—the R8520-406 manufactured by HAMAMATSU Photonics — is used for the detection of scintillation and EL photons whose wavelength is peaked at ∼170 nm. The effective area of the photocathode of the PMT is 20.5 mm × 20.5 mm. Meshes are placed at the bottom of the drift and EL region, and are named drift mesh and EL mesh, respectively. The woven-type drift and EL meshes are made of gold-plated tungsten wires whose diameter is 0.03 mm and pitch is 100 wires/in. In this paper, the cathode of the TPC is referred to as the drift top. The potential of the drift top is fixed to the ground level, and positive voltages are applied to the meshes to form the electric fields. To shield the −800 V potential applied to the PMT surface, a ground level mesh is placed 3 mm above the PMT. The insulators supporting the electrodes are made of polytetrafluoroethylene (PTFE) with a 20-mm-diameter hole, so as to increase the scintillation yield by reflecting VUV photons. Ionized electrons move in the drift region toward the EL region, where they generate EL photons. The z-axis corresponds to the direction of the drift electric field; in this paper, the direction along the electric field is called vertical and that perpendicular to the

2018 JINST 13 P07015

electric field is called horizontal. Figure 2 shows the electric field calculated using gmsh [4] and Elmer [5]. Because of the leakage of the EL field to the drift region, the drift electric field strength is higher than the expected strength based on the potential difference between the drift top and the drift mesh: 6.6 V/cm/atm instead of 4 V/cm/atm when +16 V and +1456 V are applied to the drift mesh and EL mesh, respectively (see left-panel inset in figure 2). In this paper, we assume values based on the simulation as the drift electric field. The effect of the drift electric field on the EL field is less than 0.3%. The electron passage rate through the drift mesh is estimated to be ~ 100% by simulating the drift motion of 100 electrons with the Garfield++ toolkit [6] when the voltage referenced above is applied.

A waveform digitizer (CAEN V1720) is used to record signals from the PMT at a sampling rate of 250 MHz. An ^{241}Am α-particle source (5.4 MeV) is set on the cathode electrode. The thickness of the source is ~ 3 nm, and the energy loss in the source is negligible. Actually, α-particles with energy differences of ~0.8% of 5485.56 keV at 84.5% and 5442.80 keV at 13.0% are generated from the source. Because the energy resolution is about 15%, the difference in energy of α-particles is not considered. The range of a 5.4 MeV α-particle is 2.7 mm in 8 atm Xe gas [7]. The gas supply and circulation system for this measurement is the same as the one used in [8]. At the time of measurement, Xe gas was circulated so as not to deteriorate the detector's performance. As the pump, PumpWorks model PW 2070, which can operate in high-pressure gas environment was used, and SAES MicroTorr-MC1-902 and API API-GETTER-I-Re were used in series for purification.

3 Measurements

Two types of measurements were performed. First, we measured the scintillation photons at several drift electric field strengths to confirm that the slow component is made of recombination photons. Because recombination is caused during the drift movement of electrons, the recombination photons are expected to be detected several μs after the de-excitation process. It is also expected the recombination rate is reduced at higher electric fields because electrons are more quickly separated from ions. Second, to measure the angular dependence of scintillation, we apply the EL electric field and obtain the event-by-event longitudinal distribution of the ionization electrons from the EL waveform. When the track is aligned to the electric field direction, more electrons are generated closer to the EL region; thus, the EL emission is expected to occur earlier.

3.1 Electric field dependence of scintillation yield

Scintillation yields are measured at several electric field settings. In this measurement, the EL field is not applied. Examples of the waveforms at electric fields of 0 and 100 V/cm/atm are shown in figure 3. More photons exist after the initial peak when the drift field is not applied. To quantify the number of photons, here, we define the fast and slow components as the photon yield in 0–0.04 μs and 0.4–10 μs, respectively. Figure 4 shows the electric field dependence of the fast and slow components. When the drift electric field is applied, the slow component decreases. This observation is consistent with the expectation that both recombination and the slow component increase at lower electric fields. This phenomenon has been reported in the literature [9, 10]. Unlike the slow component, the fast component has no dependence on the drift electric field. The fast component is considered to be de-excitation photons from excited Xe atoms by an α-particle,

2018 JINST 13 P07015

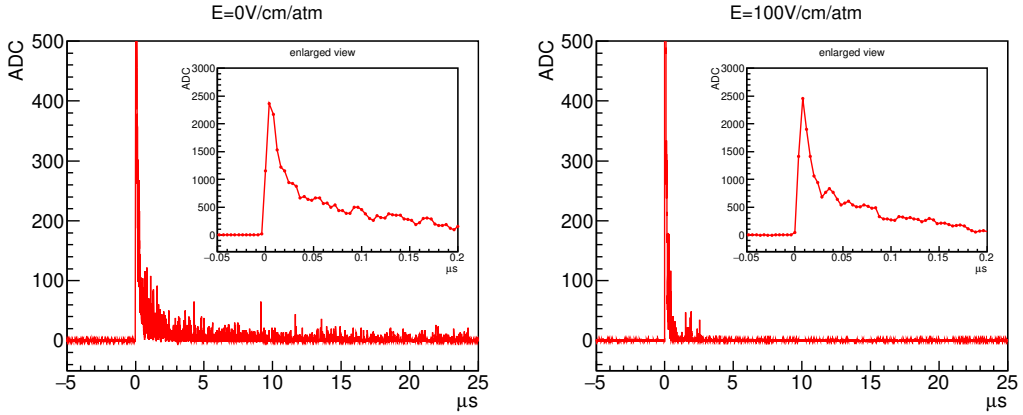

Figure 3. Examples of observed waveforms of the scintillation signal by a 5.4 MeV α-particle when the drift electric field is 0 V/cm/atm (left graph) and 100 V/cm/atm (right graph). Time zero is defined as the rise time of the scintillation waveform.

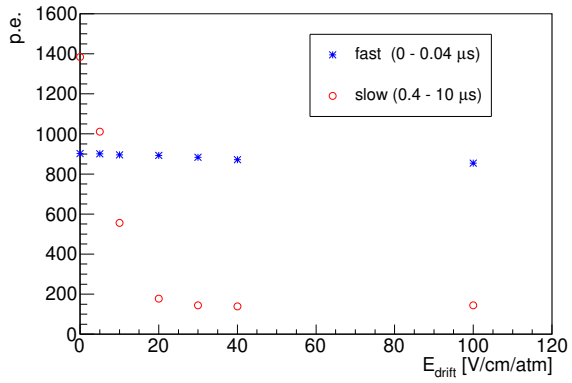

Figure 4. Drift electric field dependence of the fast (0–0.04 μs) and slow (0.4–10 μs) scintillation components.

mainly through the following process: one excited Xe atom collides with another atom and creates an excited molecule, which emits one photon [11]. The slight negative slope of the fast component is thought to be due to a small contribution from the recombination photons.

3.2 Angular dependence of scintillation and ionization electron yields

To measure the angular dependence of the scintillation yield, we apply the EL electric field. Figure 5 shows waveform examples when 6.6 and 900 V/cm/atm are applied to the drift and EL regions, respectively. The ionization electrons drift to the EL region and generate EL photons; hence, the ionization electrons are observed after the scintillation photons. Because the electrons generated closer to the EL region reach that region earlier, the time profile of the EL photons represents the ionization electron distribution projected to the z-axis. In the left graph of figure 5, there are more photons observed early on. This result reflects the Bragg curve: the α-particle is emitted from the drift top and stops at a position closer to the EL field.

2018 JINST 13 P07015

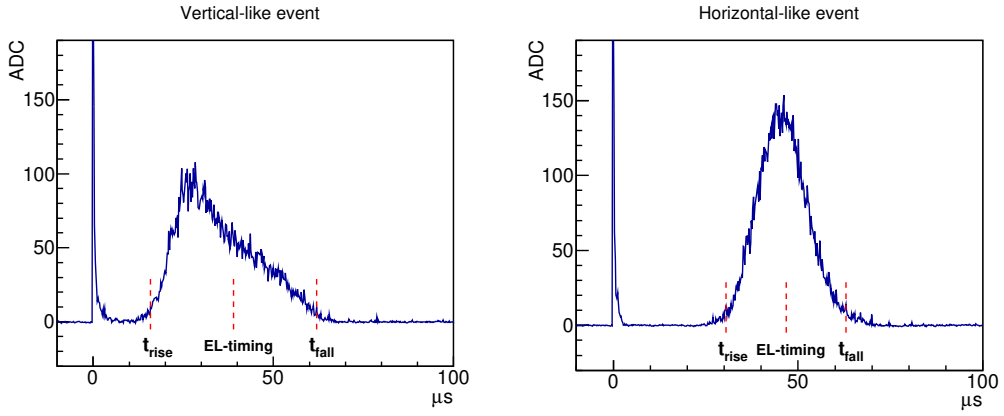

Figure 5. Examples of the measured waveforms when 6.6 V/cm/atm is applied to the drift electric field and 900 V/cm/atm is applied to the EL field. EL photons are observed after the scintillation photons. The time profile of the EL waveform represents the ionization electron distribution along the z-axis. The left and right graphs are typical waveforms when the *EL-timing* parameter is early and late, respectively. The red dashed lines show the rise and fall time.

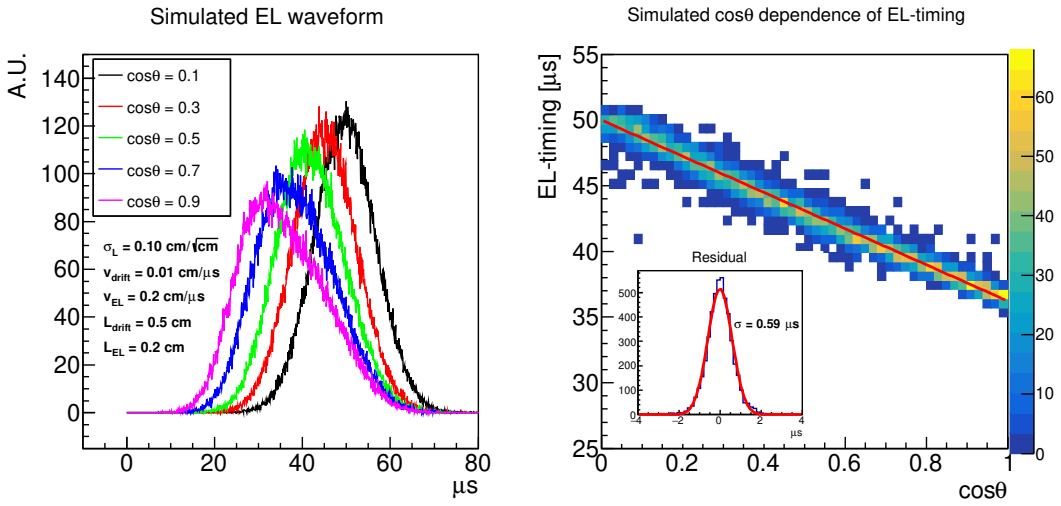

Figure 6. Graphs showing the simulated EL waveforms for several $\cos\theta$ (left) and the simulated $\cos\theta$ dependence on the *EL-timing* parameter (right). Time 0 is the start time of the event, which corresponds to the rise time of the scintillation signal in the experimental data. The straight red line is a fitted one, and the inset shows the residual of the histogram and the line. θ is the angle of an α-particle direction measured from the drift direction, as drawn in figure 1. In the simulation, the drift velocity of the drift region is set to 0.01 cm/µs and that of the EL region is set to 0.2 cm/µs; the longitudinal diffusion coefficient is set to 0.1 cm/$\sqrt{\text{cm}}$.

We define the parameter *EL-timing* as

$$EL\text{-}timing = \frac{t_{\text{rise}} + t_{\text{fall}}}{2}, \tag{3.1}$$

where t_{rise} and t_{fall} are the rise and fall time of the EL signal, which are determined as follows: rebin the waveform 50 times coarser (corresponding to a 5 MHz sampling rate), set the threshold

2018 JINST 13 P07015

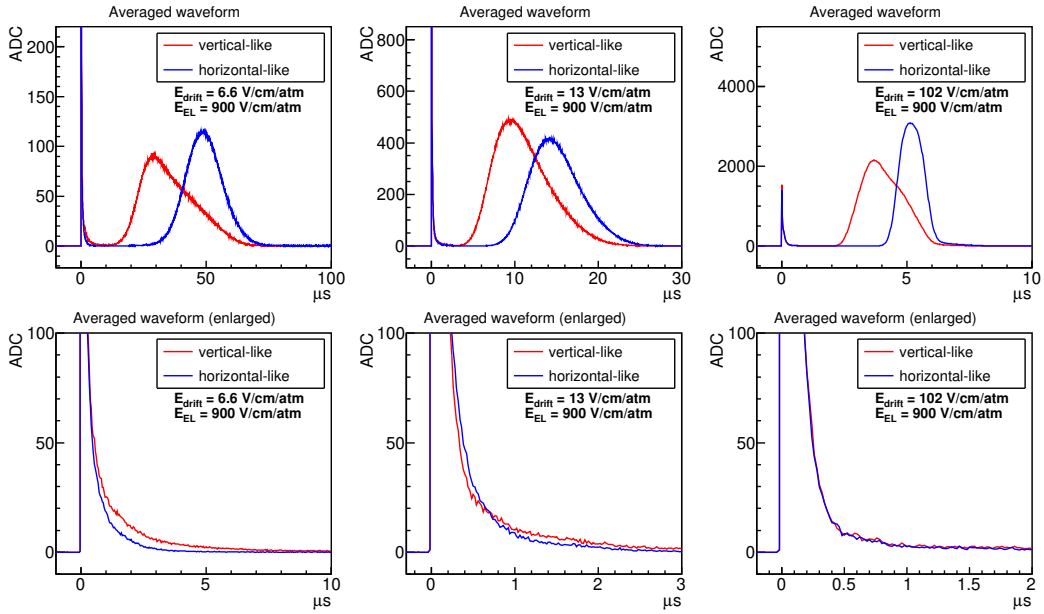

Figure 7. Measured averaged waveforms of the scintillation and EL signal for 6.6, 13, and 102 V/cm/atm of the drift electric field. Blue lines are the average of events from the largest 20% of the *EL-timing* distributions and correspond to the horizontal track; red lines are the average of events from the smallest 20% of the *EL-timing* distributions and correspond to the vertical track. The plots show waveforms in a wide range so that the EL signal can be seen, and the bottom plots show them in a narrow range, where the scintillation signal is dominant.

value at 8% of the peak height, and find the time at which the signal crosses the threshold. The calculated $t_{\rm rise}$, $t_{\rm fall}$ and *EL-timing* are shown in figure 5 as red dashed lines. Because the start point of the α-particle track is fixed to the drift top, the *EL-timing* is expected to depend linearly on $\cos\theta$ of the α-particle, where θ is measured from the drift direction ($-z$ direction). The diffusion and distribution of electrons would affect this dependence. We perform a simulation study to estimate this effect. We generate α-particles to obtain the z distribution of ionization electrons by the Geant4 simulation platform [12]. The drift velocity and longitudinal diffusion constant are tuned such that the distributions of $t_{\rm rise}$ and $t_{\rm fall}$ match observed values. The obtained drift velocity and diffusion constant are 0.01 cm/μs and 0.1 cm/$\sqrt{\rm cm}$, respectively, and consistent with the measured values in [13–15]. The left graph in figure 6 shows simulated EL waveforms, and the waveform with early *EL-timing* corresponds to a larger $\cos\theta$ (vertical direction) event. The right graph in figure 6 shows the correlation between *EL-timing* and $\cos\theta$ obtained by the simulation. There is linearity between *EL-timing* and $\cos\theta$ even with diffusion. By considering the residuals of the histogram and the straight line, we estimate the uncertainty to be 0.59 μs. Therefore, we use *EL-timing* as a parameter to represent the angle of the α-particle.

Figure 7 shows the measured waveforms averaged over many pulses. Event selections using *EL-timing* are made to select horizontal or vertical tracks. Events from the smallest 20% of the *EL-timing* distributions are taken as vertical events, while those from the largest 20% are taken as horizontal events. The actual cut values are shown in table 1. It can be seen that more photons are detected up to 10 μs for the vertical-like track with 6.6 V/cm/atm of the drift electric field — an observation expected with columnar recombination. The timescale of the scintillation emission is

2018 JINST 13 P07015

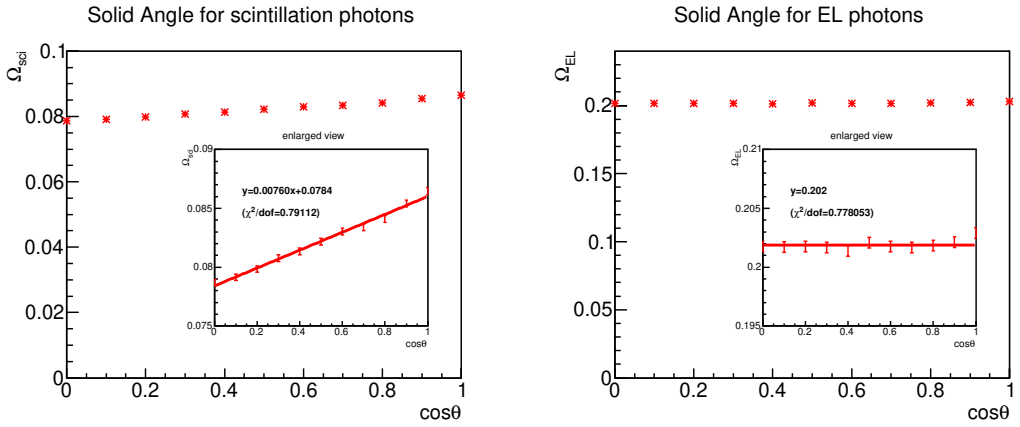

Figure 8. Simulated solid angle of the PMT given as a function of $\cos\theta$, where θ is the angle of α-particle. The reflection on the PTFE insulator (66%) and drift top (20%) and the aperture ratio of the meshes (77.8%) are taken into account. The error bars are statistical ones. The straight lines are fitted to the data with a linear function (left) and a constant function (right).

consistent with that of ionization electrons overlapping with Xe ions. For vertical tracks, it takes 30 µs for the electrons to drift the α-particle track length. At 13 V/cm/atm, a similar tendency to that at 6.6 V/cm/atm is observed for the scintillation signal after 0.6 µs, but not before 0.6 µs — the yield is less for vertical-like tracks. The reason for this phenomenon is not known. The phenomenon itself is interesting, but because the understanding is insufficient, data measured at 13 V/cm/atm are not used in the angular dependence analysis. At 102 V/cm/atm, there is no difference in scintillation waveforms and almost all ionization electrons are considered to be drifting. On the basis of these observations, the data at a drift electric field of 6.6 V/cm/atm are used for the analysis of columnar recombination. The data recorded at 102 V/cm/atm are also shown for comparison with the case where columnar recombination does not occur. As noted in section 3.1, the fast component integration range is set to 0–0.04 µs with little recombination contamination. For 6.6 V/cm/atm (102 V/cm/atm) of the drift electric field, the slow component range is set to 0.4–10 µs (0.4–2 µs). The EL yield is calculated from the integration of 10–100 µs (2–10 µs) of the signal.

The $\cos\theta$ dependence on the solid angle of the PMT for scintillation photons ($\Omega_{\rm sci}$) and EL photons ($\Omega_{\rm EL}$) is estimated by simulation and shown in figure 8. Because vertical tracks emit their scintillation photons near the PMT, the solid angle is larger than that of the horizontal tracks; the difference is about 10%. We correct the scintillation yields (fast and slow components) using a linear function obtained through the simulation. On the other hand, $\Omega_{\rm EL}$ does not depend on $\cos\theta$, and we do not correct the EL yield.

The left plot of figure 9 shows the measured *EL-timing* dependence on the EL yield when 102 V/cm/atm is applied as the drift field, where recombination is expected to be marginal. The upper horizontal axes show corresponding $\cos\theta$ values. Though it is expected that there is no angle dependence on the EL yield, the EL yield is smaller for longer *EL-timing* events. There are two possibilities for the *EL-timing* dependence on EL yield. The first possibility is the attachment: the number of electrons decreases as *EL-timing* increases. In this case, it is necessary to correct the EL yield to determine the number of ionized electrons, and columnar recombination will be

2018 JINST 13 P07015

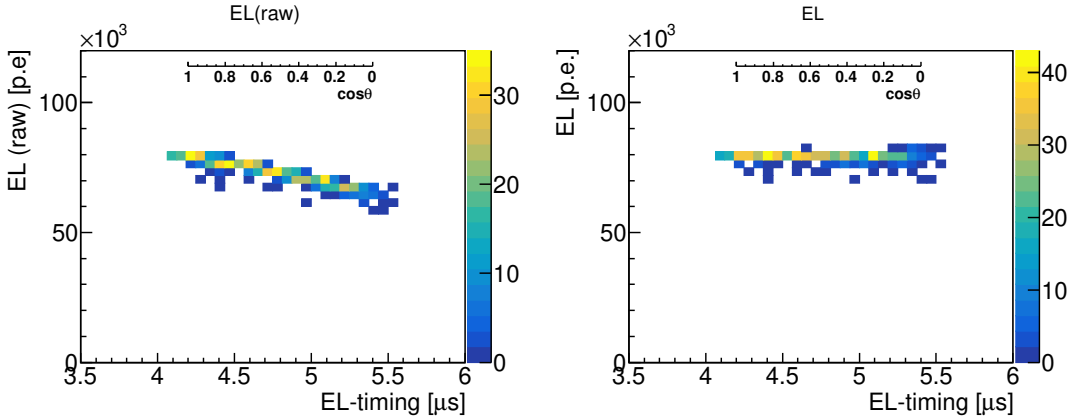

Figure 9. The left figure shows the measured *EL-timing* dependence of EL photon yield when 102 V/cm/atm (900 V/cm/atm) is applied as the drift (EL) electric field. Corresponding $\cos\theta$ values are drawn inside the plot. The right figure is the same but after the correction.

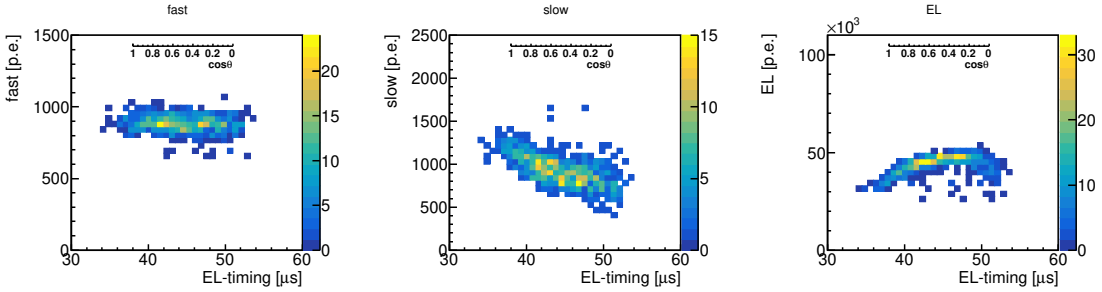

Figure 10. *EL-timing* dependence on the number of photons detected. From left to right, the three plots correspond to the fast component, slow component, and the EL signal. The drift electric field is applied at 6.6 V/cm/atm, and the EL one at 900 V/cm/atm.

enhanced because the EL yield is increased in the horizontal events. The second possibility is that ionization electrons collide with the drift top and are missing. Because there is an α-particle source on the drift top, the influence of electron loss is particularly large for the horizontal tracks. In this case, not only the EL yield but also the slow component should be corrected in the same way. Columnar recombination is enhanced on the EL signal but degraded on the slow component signal. Measurement of the attachment with another detector [8] using the same gas circulation system as that used for this measurement reveals that the electron lifetime is 5 ms or more. This result indicates that the loss of electrons is 1% or less, even with a drift of 50 μs. Given that the detector contents and outgas are different, the electron lifetime for this measurement is not necessarily the same; however in this measurement, the attachment might not be influential. Therefore, the latter model is adopted as a pessimistic scenario for columnar recombination, and both the EL yield and slow component are corrected by a $\cos\theta$ function such that the angular dependence of the EL yield at the high electric field becomes flat, as shown in the right plot of figure 9.

The *EL-timing* dependence of the fast, slow and EL yields measured at 6.6 V/cm/atm of the drift electric field are shown in figure 10. The numerical values are shown in table 1. The fast

2018 JINST 13 P07015

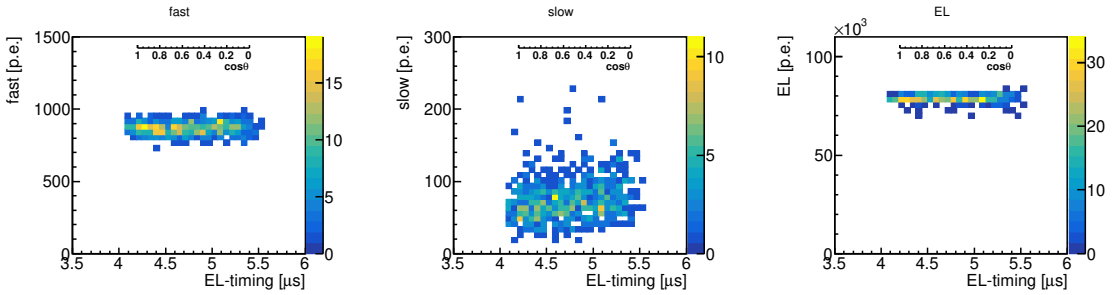

Figure 11. Same plot as those shown in figure 10, but the drift electric field applied at 102 V/cm/atm.

Table 1. Photon yields when the drift electric field is 6.6 V/cm/atm. Events with 20% from the smaller (larger) *EL-timing* were taken as vertical (horizontal) events. Concrete values are as shown in the table.

	vertical track [p.e.] (*EL-timing* < 40.90 μs)	horizontal track [p.e.] (*EL-timing* > 48.35 μs)
fast (0–0.04 μs)	897 ± 47	874 ± 59
slow (0.4–10 μs)	1129 ± 117	805 ± 151
EL (10–100 μs)	38765 ± 3763	44123 ± 4873

Table 2. Photon yields when the drift electric field is 102 V/cm/atm.

	vertical track [p.e.] (*EL-timing* < 4.370 μs)	horizontal track [p.e.] (*EL-timing* > 5.102 μs)
fast (0–0.04 μs)	873 ± 33	875 ± 43
slow (0.4–2 μs)	70 ± 33	84 ± 26
EL (2–10 μs)	79008 ± 877	79197 ± 1928

component, corresponding to the de-excitation of Xe atoms excited by an α-particle, shows no dependence on *EL-timing*. The slow component, which represents the number of recombination photons, shows a negative correlation. The EL yield representing the ionization electrons shows a positive correlation. These correlations indicate the presence of an angular-dependent columnar recombination. Thus, the energy and angle of α-particle can be reconstructed from the scintillation time profile and ionization signal. The angular resolution obtained from the residual when fitting the correlation between the slow component and the angle θ to a straight line is 40 degree (FWHM).

Figure 11 shows the *EL-timing* dependence of the number of photons detected when the drift electric field is increased to 102 V/cm/atm. The numerical values are shown in table 2. The yield of the fast component is similar to that in figure 10, and consistent with the fact that the de-excitation process does not depend on the electric field strength. The slow component is smaller than that shown in figure 10, and the EL yield is larger. In addition, a much weaker angular dependence is observed. This result indicates that columnar recombination is suppressed at higher electric fields.

2018 JINST 13 P07015

4 Conclusion

We investigated the angular dependence of columnar recombination in Xe gas with 5.4 MeV α-particles. An electric field was applied, and the time profile of the scintillation signal was used to extract the fast and slow components. The ionization signal was measured using the EL signal. The track angle θ was reconstructed from the *EL-timing* parameter, and the angular dependence of the signals was measured. While the fast component showed no angular dependence, we observed that the slow component increased and ionization signals decreased for tracks parallel to the electric field. Our result indicates that both the energy and angle can be reconstructed from the time profile of the scintillation light. This phenomenon, if established for lower energy nuclear recoil, will open the possibility of conducting a direction-sensitive dark matter search with a large mass detector.

Acknowledgments

This work was supported by the Japan Society for the Promotion of Science (JPSP) Grant-in-Aid for Scientific Research on Innovative Areas, Grant Number 15H01034.

References

[1] D.R. Nygren, *Columnar recombination: a tool for nuclear recoil directional sensitivity in a xenon-based direct detection WIMP search*, *J. Phys. Conf. Ser.* **460** (2013) 012006.

[2] D. Herrera, S. Cebrián, T. Dafni, J. García, J. Garza, A. Goldschmidt et al., *Study of Columnar Recombination in Xe+trymethilamine Mixtures using a Micromegas-TPC*, PoS(TIPP2014)057.

[3] Y. Nakajima, A. Goldschmidt, H.S. Matis, D. Nygren, C. Oliveira and J. Renner, *Measurement of scintillation and ionization yield with high-pressure gaseous mixtures of Xe and TMA for improved neutrinoless double beta decay and dark matter searches*, *J. Phys. Conf. Ser.* **650** (2015) 012012 [arXiv:1505.03585].

[4] C. Geuzaine and J.-F. Remacle, *Gmsh: A 3-D finite element mesh generator with built-in pre- and post-processing facilities*, *Int. J. Numer. Meth. Eng.* **79** (2009) 1309.

[5] https://www.csc.fi/web/elmer/.

[6] https://garfieldpp.web.cern.ch/garfieldpp/.

[7] J.F. Ziegler and J.P. Biersack, *SRIM — The Stopping and Range of Ions in Matter*, http://www.srim.org (1985).

[8] S. Ban et al., *Electroluminescence collection cell as a readout for a high energy resolution Xenon gas TPC*, *Nucl. Instrum. Meth.* **A 875** (2017) 185 [arXiv:1701.03931].

[9] S. Kobayashi et al., *Scintillation luminescence for high-pressure xenon gas*, *Nucl. Instrum. Meth.* **A 531** (2004) 327.

[10] M. Mimura, S. Kobayashi, T. Ishikawa, M. Miyajima and N. Hasebe, *Intensity and time profile of recombination luminescence produced by an alpha-particle in dense xenon gas*, *Nucl. Instrum. Meth.* **A 613** (2010) 106.

[11] K. Saito, S. Sasaki, H. Tawara, T. Sanami and E. Shibamura, *Simultaneous measurements of absolute numbers of electrons and scintillation photons produced by 5.49 MeV alpha particles in rare gases*, *IEEE Trans. Nucl. Sci* **50** (2003) 2452.

2018 JINST 13 P07015

[12] GEANT4 collaboration, S. Agostinelli et al., *GEANT4: A Simulation toolkit*, *Nucl. Instrum. Meth.* **A 506** (2003) 250.

[13] J.L. Pack, R.E. Voshall and A.V. Phelps, *Drift Velocities of Slow Electrons in Krypton, Xenon, Deuterium, Carbon Monoxide, Carbon Dioxide, Water Vapor, Nitrous Oxide, and Ammonia*, *Phys. Rev. 127* (1962) 2084.

[14] H. Kusano, J.A. Matias-Lopes, M. Miyajima, E. Shibamura and N. Hasebe, *Density Dependence of the Longitudinal Diffusion Coefficient of Electrons in Xenon*, *Jpn J. Appl. Phys.* **51** (2012) 048001.

[15] H. Kusano, J.A. Matias-Lopes, M. Miyajima, E. Shibamura and N. Hasebe, *Electron Mobility and Longitudinal Diffusion Coefficient in High-Density Gaseous Xenon*, *Jpn J. Appl. Phys.* **51** (2012) 116301.

2018 JINST 13 P07015